



NIH Public Access

Author Manuscript

Proteins. Author manuscript; available in PMC 2013 June 01.

Published in final edited form as:
Proteins. 2012 June ; 80(6): 1620–1632. doi:10.1002/prot.24056.

Simulations of substrate transport in the multidrug transporter EmrD

Joseph Baker³, Stephen H Wright², and Florence Tama¹

¹Department of Chemistry and Biochemistry The University of Arizona 1041 E. Lowell Street Tucson, AZ, 85721 USA

²Department of Physiology The University of Arizona 1656 E Mabel Ave Tucson, AZ 85724 USA

³Department of Physics The University of Arizona 1118 E Fourth Street Tucson, AZ 85721 USA

Abstract

EmrD is a multidrug resistance (MDR) transporter from *Escherichia coli*, which is involved in the efflux of amphipathic compounds from the cytoplasm, and the first MDR member of the major facilitator superfamily (MFS) to be crystallized. Molecular dynamics simulation of EmrD in a phospholipid bilayer was used to characterize the conformational dynamics of the protein.

Motions that support a previously proposed lateral diffusion pathway for substrate from the cytoplasmic membrane leaflet into the EmrD central cavity were observed. Additionally, the translocation pathway of metachloro carbonylcyanide phenylhydrazone (CCCP) was probed using both standard and steered molecular dynamics simulation. In particular, interactions of a few specific residues with CCCP have been identified. Finally, a large motion of two residues, Val 45 and Leu 233, was observed with the passage of CCCP into the periplasmic space, placing a lower bound on the extent of opening required at this end of the protein for substrate transport. Overall, our simulations probe details of the transport pathway, motions of EmrD at an atomic level of detail, and offer new insights into the functioning of MDR transporters.

Keywords

membrane transporter; steered molecular dynamics; major facilitator superfamily Work performed at University of Arizona

INTRODUCTION

EmrD is a member of the major facilitator superfamily (MFS) of membrane transporter proteins,¹ the largest family of secondary transporters.² EmrD is involved in the efflux of a structurally diverse array of amphipathic compounds from the cytoplasm towards the periplasm.^{3,4} The ability to transport a variety of substrates is a common characteristic of multidrug resistance (MDR) proteins, of which EmrD is an example.⁵ Since EmrD is a secondary transporter, it relies on a solute concentration gradient (for EmrD a proton concentration gradient) instead of the use of ATP hydrolysis to drive the conformational changes necessary for the transport of substrate along its central translocation pathway. EmrD is one of only three members of the MFS that have had structures determined by x-ray crystallography. Unlike the two other MFS proteins with available crystal structures (LacY⁶ and GlpT⁷), EmrD's interior is mostly hydrophobic, consistent with its role as a

Corresponding author: Florence Tama, Department of Chemistry and Biochemistry, The University of Arizona, 1041 E. Lowell Street, Tucson, AZ, 85721, USA. Phone: 1-520-626-4725, Fax: 1-520-621-8407, ftama@u.arizona.edu.

transporter of amphipathic molecules.⁸ The transition between the open and closed forms for members of the MFS is proposed to occur via the alternating access, “rocker-switch” mechanism,² which is supported by recent biochemical studies on LacY.^{9–12} In this mechanism, conformational changes of the central water-filled cavity (the cleft between the N- and C-terminal halves of an MFS protein) expose a substrate binding pocket to either the cytoplasm or the periplasm, but not to both simultaneously. While the crystal structures of LacY and GlpT appear to be in a shape distinctly open to the cytoplasm, EmrD is straighter and less V-shaped suggesting an intermediate occluded conformation between the open and closed forms of the protein.⁸

The ability of MDR proteins to recognize and transport a wide spectrum of molecules is believed to be related to their large and flexible central cavities that could provide different substrates with many options for orientations and interactions to satisfy shape complementarity.^{13,14} One class of drugs which EmrD expels act as uncouplers of oxidative phosphorylation.³ These drugs, which are weak lipophilic acids, can diffuse directly across the cell membrane from the periplasmic space to the cytoplasmic space and deposit ionisable protons in the cytosol, thus draining the energy stored in the proton concentration gradient that secondary active transporters require to function.¹⁵ MDR members of the MFS, like EmrD, appear to have the ability to expel substrate from either the cytoplasm, or the inner membrane leaflet.^{16–21} By removing substrate from the membrane directly, EmrD would be able to prevent depletion of the proton concentration gradient by not allowing the drug to deposit its proton in the cytoplasm. A region at the cytoplasmic end of helix 4 (H4) which includes charged residues has been proposed to be part of a “selectivity filter” involved in intake of substrate from the inner membrane leaflet in EmrD.⁸

Currently, very little is known about the specific role of the various amino acids at the cytoplasmic surface of EmrD or within the central cavity (the substrate translocation pathway) for the transport process. EmrD is homologous, about 40% similarity, to other MDR MFS proteins such as NorA, LmrP, FloR, Bmr, MdfA and Bcr.^{5,8} While EmrD has not been well characterized, biochemical studies have been carried out on several of its homologues.^{16,17} Substrate interactions with aromatic residues in multidrug-binding proteins have been shown to be important.^{22–25} In EmrD, the transmembrane (TM) helices forming the central cavity are lined with hydrophobic residues; in particular two pairs of aromatic residues found in the central cavity (Tyr 52/Tyr 56 as well as Trp 300/Phe 249) have been suggested to play a role in interacting with aromatic substrates through ring stacking.⁸ Charged residues on the cytoplasmic side of EmrD may have a role in substrate recognition.⁸ In MdfA, residues important for substrate binding were identified in the cytoplasmic halves of helices 4, 5 and 6.²⁶ Additionally, cysteine mutations on helix 10 and the loop connecting helices 10 and 11 in MdfA cause significant decrease in its ability to function as a multidrug transporter.²⁷ Other studies indicate that some of the MDR members have more than one drug interaction site and could bind multiple substrates simultaneously.^{28–30} Such a mechanism has been shown for the soluble multidrug-binding protein, QacR; its crystal structure revealed two substrates within the binding cavity.²²

Though EmrD is poorly biochemically characterized, it is one of the rare proteins with an available structure for MDR transporters. A number of EmrD amino acid residues have been suggested to play a role in the substrate transport process based on both their characteristics, and their locations in the protein.⁸ Nevertheless, no biochemical studies have been performed to examine the details of the residues involved in transport along the central cavity, or how lateral filtration of substrate from the inner membrane leaflet might occur. Based on the x-ray structure of EmrD, questions regarding the interplay between protein dynamics and substrate transport can be investigated. Computational techniques such as molecular dynamics (MD) simulations can be used to study dynamics and to probe a

possible transport pathway for EmrD substrate in order to identify important interactions in the central cavity, thereby providing information on how this class of proteins functions.

MD simulations have been used in numerous studies to investigate proteins embedded into a lipid bilayer, including channel and pore proteins.³¹ Simulations of LacY and GlpT have probed the stability of their helices^{32,33} as well as their dynamics in both the presence and the absence of their respective substrates.^{34–38} While the timescale accessible to MD simulation is limited, steered MD (SMD) has been successfully used to investigate the pathway of a substrate through protein channels.^{39–41} By applying a steering force to selected atoms, the exploration of biological processes occurring on long time scales is computationally accessible. SMD can provide an atomic picture of interactions that occur between the protein and substrate during transport.^{35,42–44} The resolution of the EmrD x-ray structure is comparable to the resolution of LacY or GlpT structures,^{6–8} for which simulation methods have provided valuable insights.^{35,38,42} Moreover, SMD has even been successfully applied to the study of substrate translocation in membrane protein homology models.^{45–47}

In this study we present the simulation results of an all-atom membrane-embedded and explicitly solvated model of EmrD. MD simulations have been conducted to investigate protein dynamics at the tens of nanoseconds timescale in the apo state. Several simulations with a substrate molecule within the central cavity were also performed in addition to SMD simulations for which substrate is steered through EmrD from the cytoplasm to the periplasm. While EmrD can transport several structurally distinct substrates, in this work its interactions with meta-chloro carbonylcyanide phenylhydrazone (CCCP) are studied.

Because of the simulation time scale, protein response to the presence of substrate in the central cavity will not yield information about the alternating access mechanism. Additionally, as EmrD is a secondary active transporter, in order to fully model substrate translocation the effects of the proton motive force should be taken into account. However, standard MD does not allow the formation or breaking of bonds for the simulation of proton transport. Although there are other methods that can be used for modeling such processes,⁴⁸ they cannot yet be applied to simulate the protein dynamics of large systems.

Furthermore, the process of proton translocation for MDR antiporters like EmrD could be fundamentally different compared to symporters such as LacY. There is no clear evidence about how protons and substrate are transported through MDR proteins, such as whether binding occurs at a single site or multiple sites, or involves acidic residues versus protonatable residues and water.^{2,16,17} As there is no indication from experimental studies which EmrD protonation state prefers the cytoplasmic or periplasmic open conformation of the protein (in contrast to LacY for example⁴⁹), it would be beyond the scope of this study to explore the dynamics of all possible EmrD protonation states. Therefore, we focused our investigation of EmrD to a single protonation state, and used SMD and force-free substrate simulations to identify relevant interactions between CCCP and EmrD along the translocation pathway.

METHODS

System Preparation

The initial structure for simulations of EmrD was obtained from the Protein Data Bank (PDB ID: 2GFP).⁸ Glu 227 was protonated in our simulations due to its high pKa value (8.52). All other amino acids were found to have pKa values consistent with them remaining in their standard protonation states. pKa calculations were performed with PDB2PQR/PROPKA,^{50–53} which determines the shift in the pKa from a model value using an empirical

formula that takes into account desolvation effects, hydrogen bonding interactions, and electrostatic interactions. A neutral pH of 7 was used in the calculations.

The protein was placed into a pre-equilibrated DOPC (1,2-dioleoyl-*sn*-glycero-3-phosphocholine) lipid bilayer.⁵⁴ The system (protein and 189 lipid molecules) was then solvated with TIP3P water using the VMD⁵⁵ Solvate plugin. 20 Na⁺ and 27 Cl⁻ ions were included to bring the system to electrostatic neutrality. This procedure resulted in a system of 69,173 atoms and of dimensions ~ 99 × 98 × 90 Å³.

Minimization, heating, equilibration and the ensuing simulations were all performed using NAMD⁵⁶ with Amber FF99SB⁵⁷ and GAFF parameter sets.^{58,59} Parameters for CCCP were developed using Antechamber,⁶⁰ Gaussian⁶¹ and RESP⁶² (see Supporting Information for details, Fig. S1, Table S1 and Table S2). The minimization, heating, and equilibration protocol is described in Supporting Information (Table S3). The heating and equilibration were carried out in the NP_γT ensemble, in which a surface tension is applied to the lipid membrane. The Surface Tension Target parameter was set to 30 dyn/cm. The final structure obtained from this procedure was used as the starting point for the apo simulations.

Simulations

A list of the simulations carried out is in Table I. A Langevin damping coefficient of 1 ps⁻¹, Langevin Piston decay time of 100 fs and Langevin Piston period of 200 fs were employed to maintain constant temperature and pressure.⁶³ Full electrostatics in the periodic system were calculated using the Particle Mesh Ewald (PME) method,⁶⁴ using a grid size of 100 Å for the x and y dimensions, and 96 Å for the z dimension. Hydrogen bonds were kept rigid, and a 2 fs integration time step was used; nonbonded interactions within the cutoff distance (12 Å cutoff with a switching function applied between 10–12 Å) were calculated every 2 fs, and a full electrostatic calculation was made every 4 fs.

In each of the apo simulations, and the SMD simulations, the initial atom velocities were different. For all SMD simulations, the initial protein/water/lipid system corresponds to a snapshot at 2 ns of the apoa simulation. CCCP was then placed into this system with its center of mass at a position of z = 14.0 Å (protein center of mass at z = 0 Å), in a region of the central cavity near the cytoplasmic ends of helices H2, H4, H10 and H11. Water within 4 Å of CCCP was removed. In order to make sure that no clashes were present in between atoms due to the placement of CCCP into the system, 1000 steps of minimization were carried out. The SMD simulations used this system as a starting point.

A pulling force constant of 7.2 kcal/mol/Å² was applied to the center of mass of CCCP. The direction of the force was set from the initial position of CCCP towards the geometric center of the alpha carbons of residues 31, 43, 229 and 235, which sit near the periplasmic exit of EmrD. The phosphorous atoms of the lipids were constrained, as well as the alpha carbons of Phe 167 in H6 and Leu 367 in H12, to prevent overall translation of the system due to the application of the steering force to CCCP in the SMD simulations. H6 and H12 are peripheral helices (i.e., outside of the translocation pathway) in EmrD, and therefore the restraint force applied to these two residues will not affect interactions of CCCP with cavity-lining amino acids. The restraint force constant used for these atoms was 100 kcal/mol/Å². In simulations v1-a and v1-b, CCCP was pulled through the central cavity towards the periplasm at a constant speed of 1 Å/ns.

Three additional simulations (30 ns each) with no forces applied to CCCP were also performed (force-free substrate simulations) (Table I). For each simulation, the initial system was extracted from simulation v1-a with CCCP at a different position along the translocation pathway. In fs-a, CCCP was toward the cytoplasmic side at z = 3.1 Å, in fs-b

CCCP was located at $z = -3.8 \text{ \AA}$, i.e. near the middle of the central cavity and in fs-c CCCP was 10 \AA further ($z = -13.7 \text{ \AA}$) toward the periplasmic side. In the force-free substrate simulations, no restraint forces were applied to the lipid phosphorous atoms or to the Phe 167/Leu 367 alpha carbons. Qualitative agreement of the interactions observed between the protein and substrate in the force-free and SMD simulations (discussed later) suggests that the use of the constraints in SMD do not influence the results.

Analysis

Cavity radius profiles—The program HOLE was used to calculate the radius of the central cavity in order to characterize its shape.⁶⁵ All images depicting the cavity profile were created using HOLE and VMD.⁵⁵

Inter-helical distances—Inter-helical distance changes were calculated between representative points defined for each of the TM helices at the cytoplasmic and periplasmic ends of EmrD.³⁶ These points were chosen as the center of mass of the Ca atoms of four residues at the cytoplasmic (periplasmic) end of each helix. The average distances were calculated over the first and last 1 ns of the simulation.

CCCP interaction energy—Interaction energies were calculated using NAMDEnergy in NAMD.⁴⁷ The electrostatic and van der Waals (vdW) interaction energies between EmrD and CCCP were calculated at 50 ps intervals. The interaction energy with individual helices was evaluated at 50 ps intervals. Interaction energies between CCCP and EmrD residues were calculated every 2 ps in the SMD simulations v1-a and v1-b, and every 20 ps in the force-free substrate simulations fs-a, fs-b and fs-c. Average interaction energies and their standard deviations were calculated over frames in which protein residues came within 3 \AA of CCCP.

RESULTS

EmrD apo simulations

To study the equilibrium dynamics of EmrD, we carried out a 76 ns simulation (apo-a) and a 50 ns simulation (apo-b) without the presence of CCCP in the cavity.

Protein stability and conformational change—Protein structure was relatively stable over the course of both apo simulations. The RMSD of the 12 TM helices remained around 3 \AA . The RMSD was taken to the initial frame of the simulation, due to a long minimization, heating, and equilibration phase (the RMSD, relative to the x-ray structure, after this procedure is $\sim 1.5 \text{ \AA}$) (Fig. S2). Secondary structure was well conserved, with the majority of the TM residues existing in alpha-helical or turn conformation (Fig. S3). No major motions between the N-ter and C-ter domains were observed, as the proposed large inter-domain motion associated with the alternating access mechanism may occur on a time scale beyond the 76 ns sampled here.

Although all 12 TM helices exhibited similar stability in both simulations, the individual N and C domains behaved differently, with the C-domain in apo-a being considerably more flexible (Fig. S2 and Fig. S4). The root mean square fluctuations of Ca atoms indicate that the differences in the flexibility of the C-domain between apo-a and apo-b comes from helix H8 (Fig. S4). Changes in helix packing in both simulations were on the order of a few angstroms (Fig. 1) at the periplasmic and cytoplasmic faces. Noticeable change occurred in distance between H1 and H7 on the periplasmic side, which increased by 6 \AA in apo-b (Fig. 1d). Tilting of the periplasmic half of H7 in apo-a and bending of H1 in apo-b caused the separation of the helices.

The largest conformational rearrangements were observed on the cytoplasmic side in apo-a. The cytoplasmic end of H8 separated from H1 to H7 (Fig. 1 a) and with respect to H10 to H12. The motion of H8 occurred early on, at 2.4 ns with residues 252 to 266 on H8 and the H8-H9 loop starting to swing outwards, eventually leading to an accessible pathway (Fig. 2), and didn't reverse. This region contains several proline and glycine residues, which can induce helix flexibility in proteins.^{32,33} After aligning the C-domain, the C α RMSD for residues 252 to 266 peaked at 10 Å. However, the internal flexibility of these residues, measured by calculating the C α RMSD after aligning just to this region, was about 2.5 to 3 Å. These RMSD values imply that while residues 252 to 266 are relatively internally stable, they go through a large collective motion with respect to the rest of the C-domain. In apo-b, in which only initial velocities were different, no major rearrangements were observed for H8, suggesting that such dynamics are not due to simulation instability, since problems in simulation stability would also induce similar rapid structure deformations in apo-b. Rather, as discussed later, the motion of H8 is proposed to be related to the lateral drug filtration mechanism assumed for MDR transporters.

Changes in helix packing led to rearrangements of the central cavity (Fig. 3). The apo simulations showed that the cavity remained closed on both sides of the membrane, with constrictions of about 1 Å radius at the periplasmic and cytoplasmic ends of EmrD as observed for the x-ray structure (Fig. 3). Additionally, the central constriction at z = 0 Å in the x-ray structure was removed over the course of minimization, heating and equilibration. During the first 1 ns of unconstrained simulation, the radius of this region was 3 Å in both apo simulations (Fig. 3).

Different effects were observed for the central cavity between the two apo simulations which started from the same initial structure with different initial velocities. In the apo-a simulation, the peak of the cavity radius profile shifted toward the periplasmic side, due to the tilting motion of H7, breaking the high degree of symmetry initially observed (Fig 3). Distance between the side chains of Ile 28 on H1 and Ala 228 on H7 increased from 5 Å to 10 Å, while Met 49, which is located on H2, reoriented out of the cavity, contributing to the larger radius of the periplasmic half. Reduction in the distance between side chains of Tyr 56 on H2 and Leu 303 on H10 contributed to the disappearance of the peak in the radius profile at the center of the cavity. In apo-b, the location of the peak in the cavity radius profile remained the same, as Ile 28, Ala 228 and Met 49 remained in close proximity, and Tyr 56 did not come close to Leu 303.

CCCP translocation and interactions within the EmrD channel

The EmrD x-ray structure was proposed to be a structural intermediate state of the alternating access mechanism (compared to the cytoplasm-facing structures of LacY and GlpT).⁸ The central cavity of EmrD lies between the N and C domains of the protein, purportedly providing a pathway for substrate transport between the cytoplasm and the periplasm.

To investigate the substrate translocation pathway, SMD simulations were performed to pull CCCP through the central cavity of EmrD from the cytoplasmic to the periplasmic end. Two simulations at 1 Å/ns pulling speed were performed, v1-a and v1-b. Additionally, in order to further characterize the interactions between CCCP and EmrD, three 30 ns simulations were carried out, fs-a, fs-b and fs-c (Table I), in which CCCP is located within the EmrD central cavity and no force is applied. These simulations were started from snapshots of the v1-a simulation and allowed us to study force-free motion of CCCP along the translocation pathway, which yielded complementary information to that obtained by SMD methods.

SMD simulations—Correlation between passage of CCCP with the cavity widening during the SMD simulations can be observed in Fig. 4. At various points along the translocation pathway, the cavity is widened by about 1 to 1.5 Å as CCCP passed through. For example, in the v1-a simulation, the cavity increased from ~ 0.6 Å to ~ 1.6 Å as CCCP passed z = 10 Å (Fig. 4 b, blue and green curves) and from ~ 0.8 Å to ~ 2 Å as CCCP passes z = -15 Å (Fig. 4 b, red and orange curves). As CCCP was pulled from the cytoplasmic side toward the periplasmic side of the protein, the central cavity underwent conformational rearrangements as measured by its radial size. As seen in the free simulation, an increase in the distance between the side chains of Ile 28 on H1 and Ala 228 on H7, as H7 moved out of the translocation pathway, shifted the peak of the cavity radius profile toward the periplasmic side, which remained wider even as CCCP was pulled through.

The size of the constriction around the periplasmic valve (z = -15 Å to z = -20 Å) increased in v1-a and v1-b as CCCP exited from the translocation pathway (Fig. 4 b and c). These changes were associated with the periplasmic end of H7, which moved further away from the helices in the N-terminal half of EmrD. This motion allowed for easier rearrangement of side chains at the periplasmic opening and in the periplasmic half of the cavity, permitting widening as CCCP exited. On the other hand, on the cytoplasmic side of the cavity the radius remained largely unchanged in both SMD simulations when CCCP first passed through the cytoplasmic constriction (Fig. 4 b and c).

Because the rate of substrate translocation in this SMD study of EmrD (about 1 event per 40 ns) was too fast to allow the protein to respond and relax to the passage of CCCP, the exploration of the “rocker-switch mechanism” that has been proposed for members of the MFS was not feasible on this time scale.⁴² However, interactions observed between CCCP and EmrD within the central cavity using SMD can bring some insights into residues involved in translocation.

CCCP/EmrD interactions—A number of EmrD amino acids have been suggested to play a role in the substrate transport process based on both their chemical characteristics, and their locations in the protein.⁸ Nevertheless, very few details are known about EmrD and the residues involved in transport. Here, the SMD simulations and force-free substrate simulations are used to reveal some aspects of the CCCP translocation pathway in EmrD.

In v1-a and v1-b, CCCP was pulled from the cytoplasmic end toward the periplasmic end of the central cavity, finally exiting into the periplasm. For fs-a, fs-b and fs-c, in which no forces were applied (Table I), CCCP (1) moved toward the periplasmic side of the cavity in both fs-a (starting closer to the cytoplasmic side) and fs-b (starting near the middle of the central cavity) and (2) moved slightly back towards the central cavity in fs-c (starting closer to the periplasmic side) (Fig. S5). Such motions are facilitated by the larger space generally observed towards the middle and periplasmic side of the central cavity in our simulations (Fig. 3 and Fig. 4).

In both v1-a and v1-b, we observed that a large number of hydrophobic residues made contact with CCCP, consistent with EmrD's role as a transporter of mainly amphipathic molecules. This was reflected by the predominantly larger vdW interaction energy of CCCP with the protein compared to the electrostatic interaction energy (Fig. S6 a and b). Interactions of CCCP with the N-domain, which was shown to be less flexible than the C-domain in both apo simulations (Fig. S2), were stronger than its interactions with the C-domain in v1-a and v1-b (Fig. 5 a–d). Particularly, the strongest interactions of CCCP in the SMD simulations were with H2, and to a lesser extent H4, in the N-domain (Fig. 5 a, c and e).

Strong electrostatic interaction energy was observed near the cytoplasmic entrance in both v1-a and v1-b (Fig. S6 a and b), where a greater number of polar and charged residues are located. These electrostatic interactions were primarily due to residues on H2, H4 and H11, as well as Asp 190. More specifically, Asp 190 and Asp 68 contributed to the large electrostatic interaction seen during the SMD simulations on the cytoplasmic end. Asp 190, located on the cytoplasmic interdomain loop, formed a long-lived hydrogen bond with CCCP at the nitrogen-attached proton. Asp 68 interacted with the hydrogens on the aromatic ring of CCCP at larger distance, leading to weaker interactions (Table II). As the free substrate simulations started from v1-a snapshots with CCCP further into the central cavity, no interactions with Asp 68 and Asp 190 were observed. We also found several Gln interacting with CCCP in the SMD and free substrate simulations such as Gln 60, which is close to the initial CCCP position, as well as Gln 21 and Gln 24 to a smaller extent (Table II).

Slightly further into the cytoplasmic half of the translocation pathway, interactions between CCCP and Arg 118, located on H4, were particularly strong in v1-a, v1-b and fs-a (Table II). Based on the x-ray structure, Arg 118 has been suggested to be involved in substrate recognition.⁸ Because CCCP was initially placed inside the cytoplasmic entrance to start the simulations, we cannot assess whether interactions with Arg 118 are necessary for driving the substrate into the translocation pathway. In fs-a, Arg 118 interacted with the nitrile groups of CCCP as the aromatic ring extended further into the cavity where four aromatic residues (Tyr 52/Tyr 56/Phe 249/Trp 300) are located (Fig. 6).

Within the central cavity, a pair of tyrosines (Tyr 52 and Tyr 56) was found to strongly interact with CCCP in the SMD simulations as well as in fs-a and fs-b (Table II). Nearly parallel stacking between the aromatic ring of CCCP with Tyr 52/Tyr 56 was observed in fs-a (Fig. 6). These types of ring-stacking interactions may be relevant for substrate binding; such aromatic interactions were found to be important for other multidrug-binding proteins.^{22–25} Weaker interactions with the other pair of stacked aromatics, Phe 249/Trp 300, were also observed in the SMD and free substrate simulations (Table II). In simulation fs-a, as the interaction energy of CCCP with Arg 118 and Tyr 56 decreased, the interaction energy of CCCP with Tyr 52 increased (Fig. 6). For Phe 249 and Trp 300 smaller changes in the interaction strength were seen.

Additionally, Met 49 interacted primarily with the aromatic ring of CCCP. As mentioned previously, along with Ala 228 and Ile 28, Met 49 appeared to play a role in controlling the size of the periplasmic side of the cavity, since it can easily orient itself into (or out of) the translocation pathway. Sequence alignment shows a methionine at the corresponding position in MdfA, while a leucine and valine were found in Bcr and Bmr respectively.⁸ Taken together, these observations would suggest that a hydrophobic residue at this position might be important for transport. Finally, toward the periplasmic exit, Leu 233 and Val 45 strongly interacted with CCCP in v1-a, v1-b and fs-c.

Exit of CCCP into the periplasmic space—SMD simulations indicated that movements of the periplasmic ends of H1, H2, H7 and H8 controlled the exit of CCCP. Residues on the H7–H8 loop went through a large motion with respect to the periplasmic end of H2 as CCCP exited (Fig. 7). As observed in the apo-a simulation, H7 bent further out of the translocation pathway at its periplasmic end in both v1-a and v1-b. Leu 233, located on the flexible H7–H8 loop, and Val 45 (periplasmic end of H2) were chosen to monitor the distance change between these parts of the protein. Both of these residues interacted strongly with CCCP (Table II). This inter-residue distance was extremely stable at about 5 Å, but increased to more than 10 Å when CCCP came into proximity. Once CCCP exited, the distance returned to 5 Å. The second peak in simulation v1-b (red curve in Fig. 7) was due

to continued contact of CCCP with Leu 233 as CCCP exited into the periplasmic space. While we cannot observe opening of the cavity at the periplasmic end in our force-free substrate simulations due to the complex nature of the alternating access mechanism (i.e., involving large conformational changes over an extended timescale, proton transfer events, etc), the SMD simulations suggest that changes in orientations of helices H1, H2, H7 and H8 control expulsion of CCCP into the periplasmic space. The observed motion in the SMD simulations would not directly coincide with motions that provide the alternating access mechanism. However the extent of separation between the end of H2 and the H7–H8 loop (Fig. 7 c) suggests a lower bound on the minimal distance necessary for CCCP to leave the cavity.

DISCUSSION

EmrD conformational change

A main characteristic of MDR transporters is a large and flexible central cavity allowing substrates to bind in different orientations and locations which could lead to the broad spectrum of molecules this class of proteins can recognize.^{13,14} Our apo simulations demonstrated such a flexible binding pocket, where natural fluctuations of a few side chains can have a considerable effect on the cavity profile, even in the absence of substrate (Fig. 3). Similarly, in our SMD simulations, the cavity displayed a range of different radii at a given z position as CCCP passed through (Fig. 4). For example, the size and shape of the periplasmic half cavity in v1-b as CCCP passed through (green to the red arrow, Fig. 4c) was similar to the end of the apo-a simulation, whereas in v1-a this region of the cavity did not open as wide compared to apo-a and v1-b (Fig. 4b). While these rearrangements do not offer insights into the mechanism of alternating access, the changes in the radius profile do represent the scale of natural fluctuations for EmrD on the 40–75 ns timescale. Such fluctuations can lead to a cavity wider than necessary for CCCP transport, as evidenced by the range of radii observed during CCCP translocation. This could indicate that EmrD is able to simultaneously accommodate multiple substrates in the central cavity, as has been demonstrated for LmrP and MdfA.^{28,29} In addition, these protein fluctuations could play a critical role in adapting the EmrD central cavity to a variety of molecules with structural diversity by positioning specific residues to provide favorable substrate contacts either through steric or aromatic interactions.

Cytoplasmic membrane leaflet entrance for substrates

Unlike GlpT or LacY, which accept substrate from the cytoplasmic or periplasmic space, it has been suggested, based on the structure and homology to other MDR MFS transporters, that EmrD could filter substrates from the inner membrane leaflet before the substrate has a chance to enter the cytoplasm.^{8,16–21} This mechanism would involve a “selectivity filter”, several charged residues at the cytoplasmic end of helix H4,⁸ as studies on MdfA and LmrP have shown that some of these residues play a role in substrate recognition.^{19,26} This would be an important feature for MDR transporters, as it would allow them to intercept harmful drugs for the bacteria before they have a chance to enter the cytoplasmic space. In simulation apo-a, as a result of the large motion of H8, a possible passage into the central cavity of EmrD was exposed in the H8/H9 region, which is adjacent to residues in the proposed selectivity filter and would not require substrates to enter the cavity along the central axis of the protein (Fig. 2). Thus, the observed large motion of H8 would support the proposed filtering mechanism from the inner membrane leaflet. There are several proline residues (Pro 252 and Pro 254 on H8, and Pro 266 on H9), as well as two glycines (Gly 259 on H8 and Gly 264 on the H8–H9 loop) that contribute greatly to TM helix flexibility. Additionally, this region of EmrD has several hydrophobic residues (Trp and Phe) all within close proximity of one another, whose side chains could allow for a large surface area of

interaction with a broad spectrum of amphipathic drugs. Therefore, these residues could be critical as EmrD intercepts drugs that diffuse across the lipid membrane.

Though both apo simulations were started with identical conditions (velocities were different), we only observed this motion in apo-a. In apo-b, relatively smaller rearrangements of H8 were seen. This implies that the motion is not a result of instability of the x-ray structure, or the failure of simulation protocol. Instead, it is an intrinsic motion that can occur stochastically during the course of substrate free dynamics in EmrD, and possibly represents a stable and accessible conformation of apo EmrD which could allow filtration of substrate from the inner membrane leaflet.

CCCP interactions with EmrD

Very little is known about residue interactions with CCCP as it is transported and released into the periplasmic space. Studies of other drug-binding proteins suggested the importance of aromatic residues for substrate interactions within the central cavity.^{22–25} Through a combination of our SMD simulations v1-a and v1-b, and our force-free substrate simulations fs-a, fs-b and fs-c, we were able to elucidate some important interactions between CCCP and EmrD, which may help to direct biochemical studies of the protein.

On the cytoplasmic side of the cavity, in the SMD simulations and in fs-a we observed strong interaction between CCCP and Arg 118 located on H4 (Table II). This interaction energy decreased as the interaction energy of CCCP with Tyr 52 increased in simulation fs-a (Fig. 6 c). Tyr 52 is further into the EmrD cavity, and its aromatic side chain interacted with the aromatic ring of CCCP as the charged Arg 118 side chain interacted with the nitrogen atoms of CCCP (Fig. 6 b). Electrostatic interaction with Arg 118 could help to stabilize CCCP in an orientation such that it can be “handed off” to the aromatic residues deeper into the central cavity. Therefore, Arg 118 may be essential for correctly orienting CCCP in the EmrD cavity.

It was suggested that ring-stacking interactions may be important for substrate binding in EmrD.⁸ This hypothesis was based upon similar interactions that have been found for other multidrug-binding proteins. For example, Phe residues are used in Bmr to recognize substrate,²³ and in QacR, a combination of aromatics and polar residues is used in its multidrug binding site.^{16,25} Our simulations supported this mechanism. Strong interactions between CCCP and Tyr 52/Tyr 56 were observed across multiple simulations (Table II), and in fs-a CCCP's aromatic ring is found in a nearly parallel orientation between both aromatic side chains of Tyr 52 and Tyr 56 (Fig. 6 a). On the other hand, interactions with Phe 249 and Trp 300 were weaker in all simulations with substrate. Trp 300 remains in an orientation that keeps its aromatic side chain mostly inaccessible to the translocation pathway. However, as EmrD transports a large variety of substrates, it is possible that Phe 249/Trp 300 are involved in a similar mechanism but for the efflux of structurally distinct molecules.

To obtain insights into the mechanism of EmrD as a proton gradient driven secondary transporter, we analyzed pKa values of ionizable residues for conformations sampled during MD simulations. Those calculations would not represent real dynamics of the protein that involves proton transport and conformational dynamics since protonation states are fixed in the MD simulations, however such analysis would provide a first indication of which residues might be involved in proton transport. Noticeable pKa shifts have been observed for a few residues. Among those previously mentioned, pKa values of Tyr 56 and Arg 118 change when the contact between them is disrupted by the passage of CCCP (Fig. S7 a and b) (Tyr 56 pKa value changes from ~10 to ~16 and Arg 118 from ~12 to ~10). For the first 20 ns of apo-a, the pKa value of Glu 227 remains around 8. Thereafter, the pKa value largely fluctuates between 6 and 10, and those changes are highly correlated with hydrogen

bonding to Asp 292 (Fig. S7 c and d). It has been hypothesized that the Glu 227 side chain could potentially reorient into or out of the central cavity and therefore possibly be involved in proton translocation.⁸ Such simultaneous shifts in the pKa's of Asp 292 and Glu 227 occur in both the substrate free simulation apo-a, and in the SMD simulation v1-b. Therefore, we cannot conclude whether these pKa changes are directly related to CCCP transport or are the result of intrinsic conformational fluctuations of EmrD. A more comprehensive study of proton transport in EmrD is beyond the scope of this study, however the current results would provide clues for further experimental and theoretical studies.

As CCCP moved towards the periplasmic space, helix H7 was found to bend slightly out of the central cavity in both v1-a and v1-b, motion also observed in simulation apo-a. The loop that links H7 to H8 moved away from the periplasmic end of H2 as CCCP exited into the periplasm, while they maintained a stable distance from one another for a majority of the simulation time (Fig. 7). The motion observed between these regions of the protein suggests a lower bound on the required distance to permit CCCP to exit from the central cavity. The H7–H8 loop has to move as CCCP is being pulled through, but it is clear that rearrangements of the periplasmic ends of H7, H8, H2 and H1 would be required to occur for CCCP to exit to the periplasm.

CONCLUSION

We have investigated the MDR membrane protein, EmrD, using MD simulations. EmrD's role as an efflux pump is implicated in the development of MDR super bacteria. Our simulations have revealed motions that may provide an entrance from the cytoplasmic membrane leaflet, in accordance with a previously proposed mechanism for substrate filtration. The stacked aromatics Tyr 52 and Tyr 56 in EmrD interacted strongly with CCCP during transport, and had nearly parallel ring-stacking interactions with CCCP in our simulations. The exit of CCCP into the periplasm involves a motion between the periplasmic end of H2 and the H7–H8 loop that increases the distance between these regions by a factor of 2, effectively establishing a lower bound on the size of the space required for the release of CCCP from the cavity.

EmrD is involved in the efflux of amphipathic molecules from the cytoplasm towards the periplasm. For a complete picture of the function of EmrD, one needs to study proton transfer, substrate translocation, and protein conformational changes, which is challenging from both an experimental and theoretical perspective. Our results provide the first information for a detailed understanding of the drug transport pathway in EmrD. Even though simulation timescales are too short to capture the full development of conformational changes of EmrD, some molecular events associated with CCCP translocation have been uncovered. These results could lead toward a more complete view of the overall mechanism of efflux of amphipathic drugs by EmrD and MDR proteins in general.

Supplementary Material

Refer to Web version on PubMed Central for supplementary material.

Acknowledgments

Financial support from the National Institute of Health, grant 2R01DK058251-09 is greatly appreciated.

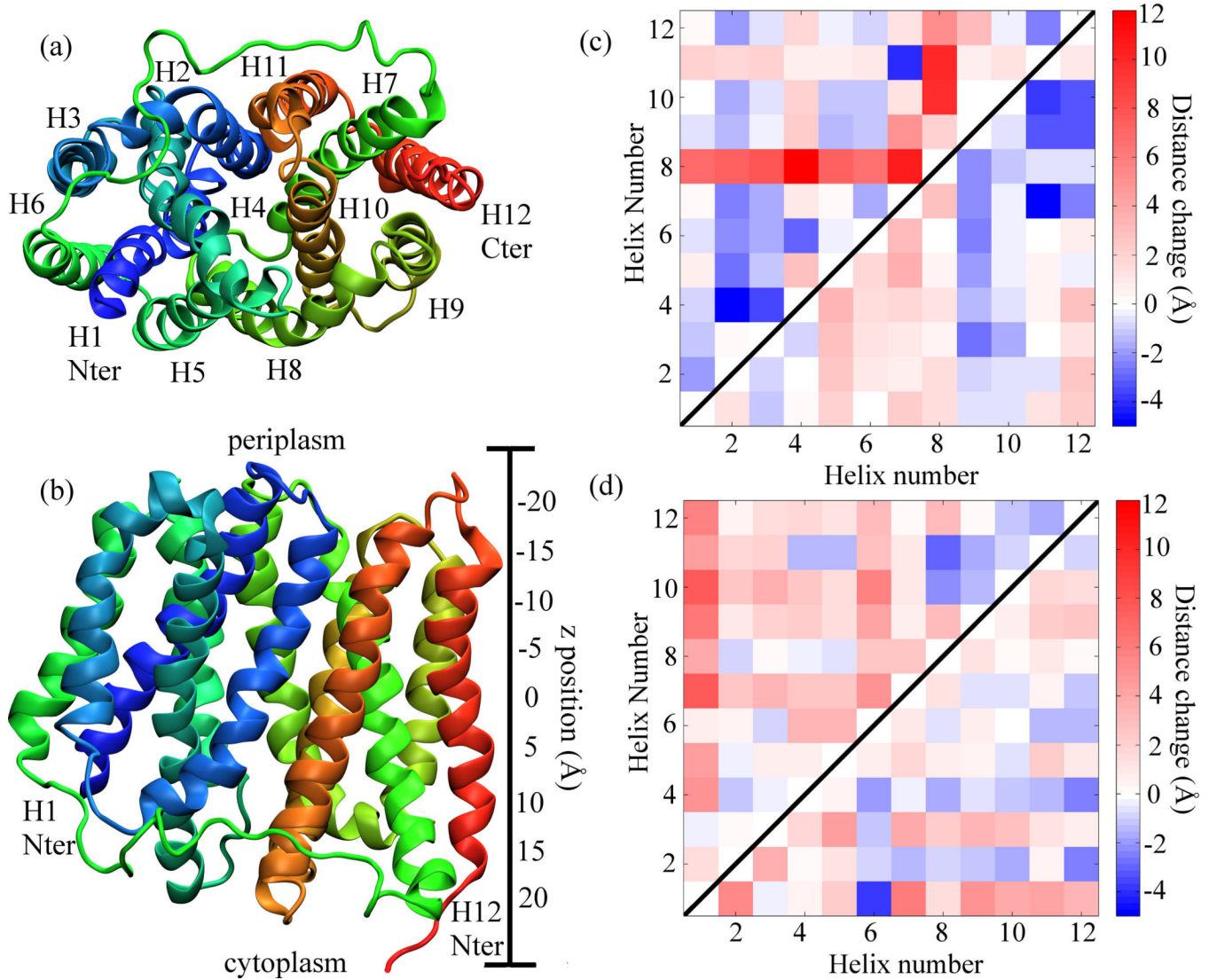
References

1. Pao SS, Paulsen IT, Saier MH Jr. Major Facilitator Superfamily. *Microbiol Mol Biol R.* 1998; 62:1–34.

2. Law CJ, Maloney PC, Wang DN. Ins and Outs of Major Facilitator Superfamily Antiporters. *Annu Rev Microbiol.* 2008; 62:289–305. [PubMed: 18537473]
3. Naroditskaya V, Schlosser MJ, Fang NY, Lewis K. An *E. coli* Gene is Involved in Adaptation to Low Energy Shock. *Biochem Biophys Res Co.* 1993; 196:803–809.
4. Nishino K, Yamaguchi A. Analysis of a Complete Library of Putative Drug Transporter Genes in *Escherichia coli*. *J Bacteriol.* 2001; 183:5803–5812. [PubMed: 11566977]
5. Paulsen IT, Brown MH, Skurray RA. Proton-Dependent Multidrug Efflux Systems. *Microbiol Rev.* 1996; 60:575–608. [PubMed: 8987357]
6. Abramson J, Smirnova I, Kasho V, Verner G, Kaback HR, Iwata S. Structure and Mechanism of the Lactose Permease of *Escherichia coli*. *Science.* 2003; 301:610–615. [PubMed: 12893935]
7. Huang Y, Lemieux MJ, Song J, Auer M, Wang DN. Structure and Mechanism of the Glycerol-3-Phosphate Transporter from *Escherichia coli*. *Science.* 2003; 301:616–620. [PubMed: 12893936]
8. Yin Y, He X, Szewczyk P, Nguyen T, Chang G. Structure of the Multidrug Transporter EmrD from *Escherichia coli*. *Science.* 2006; 312:741–744. [PubMed: 16675700]
9. Kaback HR, Dunten R, Frillingos S, Venkatesan P, Kwaw I, Zhang W, Ermolova N. Site-directed alkylation and the alternating access model for LacY. *P Natl Acad Sci USA.* 2007; 104:491–494.
10. Majumdar DS, Smirnova I, Kasho V, Nir E, Kong X, Weiss S, Kaback HR. Single-molecule FRET reveals sugar-induced conformational dynamics in LacY. *P Natl Acad Sci USA.* 2007; 104:12640–12645.
11. Smirnova I, Kasho V, Choe JY, Altenbach C, Hubbell WL, Kaback HR. Sugar binding induces an outward facing conformation of LacY. *P Natl Acad Sci USA.* 2007; 104:16504–16509.
12. Zhou Y, Guan L, Freites JA, Kaback HR. Opening and closing of the periplasmic gate in lactose permease. *P Natl Acad Sci USA.* 2008; 105:3774–3778.
13. Neyfakh AA. Mystery of multidrug transporters: the answer can be simple. *Mol Microbiol.* 2002; 44:1123–1130. [PubMed: 12068801]
14. Lewinson O, Adler J, Sigal N, Bibi E. Promiscuity in multidrug recognition and transport: the bacterial MFS Mdr transporters. *Mol Microbiol.* 2006; 61:277–284. [PubMed: 16856936]
15. Krulwich TA, Quirk PG, Guffanti AA. Uncoupler-Resistant Mutants of Bacteria *Microbiol Rev.* 1990; 54:52–65.
16. Fluman N, Bibi E. Bacterial multidrug transport through the lens of the major facilitator superfamily. *Biochim Biophys Acta.* 2009; 1794:738–747. [PubMed: 19103310]
17. Higgins C. Multiple molecular mechanisms for multidrug resistance transporters. *Nature.* 2007; 446:749–757. [PubMed: 17429392]
18. Bolhuis H, van Veen HW, Molenaar D, Poolman B, Driessens AJM, Konings WN. Multidrug resistances in *Lactococcus lactis*: evidence for ATP-dependent drug extrusion from the inner leaflet of the cytoplasmic membrane. *EMBO J.* 1996; 15:4239–4245. [PubMed: 8861952]
19. Mazurkiewicz P, Konings WN, Poelarends GJ. Acidic Residues in the Lactococcal Multidrug Efflux Pump LmrP Play Critical Roles in Transport of Lipophilic Cationic Compounds. *J Biol Chem.* 2002; 277:26081–26088. [PubMed: 11994308]
20. Bolhuis H, van Veen HW, Brands JR, Putman M, Poolman B, Driessens AJM, Konings WN. Energetics and Mechanism of Drug Transport Mediated by the Lactococcal Multidrug Transporter LmrP. *J Biol Chem.* 1996; 271:24123–24128. [PubMed: 8798651]
21. Mitchell BA, Paulsen IT, Brown MH, Skurray RA. Bioenergetics of the Staphylococcal Multidrug Export Protein QacA. *J Biol Chem.* 1999; 274:3541–3548. [PubMed: 9920900]
22. Schumacher MA, Miller MC, Brennan RG. Structural mechanism of the simultaneous binding of two drugs to a multidrug-binding protein. *EMBO J.* 2004; 23:2923–2930. [PubMed: 15257299]
23. Klyachko KA, Schuldiner S, Neyfakh AA. Mutations Affecting Substrate Specificity of the *Bacillus subtilis* Multidrug Transporter Bmr. *J Bacteriol.* 1997; 179:2189–2193. [PubMed: 9079903]
24. Zheleznova EE, Markham PN, Neyfakh AA, Brennan RG. Structural basis of multidrug recognition by BmrR, a transcription activator of a multidrug transporter. *Cell.* 1999; 96:353–362. [PubMed: 10025401]

25. Murray DS, Schumacher MA, Brennan RG. Crystal Structures of QacR-Diamidine Complexes Reveal Additional Multidrug-binding Modes and a Novel Mechanism of Drug Charge Neutralization. *J Biol Chem.* 2004; 279:14365–14371. [PubMed: 14726520]
26. Adler J, Bibi E. Determinants of substrate recognition by the *Escherichia coli* multidrug transporter MdfA identified on both sides of the membrane. *J Biol Chem.* 2004; 279:8957–8965. [PubMed: 14688269]
27. Adler J, Bibi E. Promiscuity in the Geometry of Electrostatic Interactions Between the *Escherichia coli* Multidrug Resistance Transporter MdfA and Cationic Substrates. *J Biol Chem.* 2005; 280:2721–2729. [PubMed: 15557318]
28. Lewinson O, Bibi E. Evidence for simultaneous binding of dissimilar substrates by the *Escherichia coli* multidrug transporter MdfA. *Biochemistry.* 2001; 40:12612–12618. [PubMed: 11601985]
29. Putman M, Koole LA, van Veen HW, Konings WN. The secondary multidrug transporter LmrP contains multiple drug interaction sites. *Biochemistry.* 1999; 38:13900–13905. [PubMed: 10529235]
30. Borst P, Zelcer N, van de Wetering K, Poolman B. On the putative co-transport of drugs by multidrug resistance proteins. *FEBS Lett.* 2005; 580:1085–1093. [PubMed: 16386247]
31. Roux B, Schulten K. Computational Studies of Membrane Channels. *Structure.* 2004; 12:1343–1351. [PubMed: 15296727]
32. Bennett M, D'Rozario R, Sansom MSP, Yeagle PL. Asymmetric Stability among the Transmembrane Helices of Lactose Permease. *Biochemistry.* 2006; 45:8088–8095. [PubMed: 16800633]
33. D'Rozario R, Sansom MSP. Helix dynamics in a membrane transport protein: comparative simulations of the glycerol-3-phosphate transporter and its constituent helices. *Mol Membr Biol.* 2008; 25:571–583. [PubMed: 19037818]
34. Enkavi G, Tajkhorshid E. Simulation of Spontaneous Substrate Binding Revealing the Binding Pathway and Mechanism and Initial Conformational Response of GlpT. *Biochemistry.* 2010; 49:1105–1114. [PubMed: 20058936]
35. Yin Y, Jensen M, Tajkhorshid E, Schulten K. Sugar Binding and Protein Conformational Changes in Lactose Permease. *Biophys J.* 2006; 91:3972–3985. [PubMed: 16963502]
36. Holyoake J, Sansom MSP. Conformational Change in an MFS Protein: MD Simulations of LacY. *Structure.* 2007; 15:873–884. [PubMed: 17637346]
37. Law CJ, Almqvist J, Bernstein A, Goetz RM, Huang Y, Soudant C, Laaksonen A, Hovmöller S, Wang DN. Salt-bridge Dynamics Control Substrate-induced Conformational Change in the Membrane Transporter GlpT. *J Mol Biol.* 2008; 378:828–839. [PubMed: 18395745]
38. Law CJ, Enkavi G, Wang DN, Tajkhorshid E. Structural Basis of Substrate Selectivity in the Glycerol-3-Phosphate Antiporter GlpT. *Biophys J.* 2009; 97:1346–1353. [PubMed: 19720022]
39. Sotomayor M, Schulten K. Molecular Dynamics Study of Gating in the Mechanosensitive Channel of Small Conductance MscS. *Biophys J.* 2004; 87:3050–3065. [PubMed: 15339798]
40. Yu J, Yool AJ, Schulten K, Tajkhorshid E. Mechanism of Gating and Ion Conductivity of a Possible Tetrameric Pore in Aquaporin-1. *Structure.* 2006; 14:1411–1423. [PubMed: 16962972]
41. Gumbart J, Schulten K. Molecular Dynamics Studies of the Archaeal Translocon. *Biophys J.* 2006; 90:2356–2367. [PubMed: 16415058]
42. Jensen M, Yin Y, Tajkhorshid E, Schulten K. Sugar Transport across Lactose Permease Probed by Steered Molecular Dynamics. *Biophys J.* 2007; 93:92–102. [PubMed: 17434947]
43. Celik L, Schiott B, Tajkhorshid E. Substrate Binding and Formation of an Occluded State in the Leucine Transporter. *Biophys J.* 2008; 94:1600–1612. [PubMed: 18024499]
44. Li J, Tajkhorshid E. A gate-free pathway for substrate release from the inward-facing state of the Na⁺-galactose transporter. *Biochim Biophys Acta.* 2011
45. Shan J, Javitch JA, Shi L, Weinstein H. The Substrate-Driven Transition to an Inward-Facing Conformation in the Functional Mechanism of the Dopamine Transporter. *PLoS ONE.* 2011; 6:e16350. [PubMed: 21298009]
46. Capener CE, Shrivastava IH, Ranatunga KM, Forrest LR, Smith GR, Sansom MSP. Homology Modeling and Molecular Dynamics Simulation Studies of an Inward Rectifier Potassium Channel. *Biophys J.* 2000; 78:2929–2942. [PubMed: 10827973]

47. Gabrielsen M, Ravna A, Kristiansen K, Sylte I. Substrate binding and translocation of the serotonin transporter studied by docking and molecular dynamics simulations. *J Mol Modeling*. 2011;
48. Wang D, Voth GA. Proton Transport Pathway in the ClC Cl⁻/H⁺ Antiporter. *Biophys J*. 2009; 97:121–131. [PubMed: 19580750]
49. Guan L, Kaback HR. Lessons from lactose permease. *Annu Rev Biophys Biomol Struct*. 2006; 35:67–91. [PubMed: 16689628]
50. Li H, Robertson AD, Jensen JH. Very Fast Empirical Prediction and Interpretation of Protein pKa Values. *Proteins*. 2005; 61:704–721. [PubMed: 16231289]
51. Bas DC, Rogers DM, Jensen JH. Very Fast Prediction and Rationalization of pKa Values for Protein-Ligand Complexes. *Proteins*. 2008; 73:765–783. [PubMed: 18498103]
52. Olsson MHM, Søndergaard CR, Rostkowski M, Jensen JH. PROPKA3: Consistent Treatment of Internal and Surface Residues in Empirical pKa Predictions. *J Chem Theory Comput*. 2011; 7:525–537.
53. Søndergaard CR, Olsson MHM, Rostkowski M, Jensen JH. Improved Treatment of Ligands and Coupling Effects in Empirical Calculation and Rationalization of pKa Values. *J Chem Theory Comput*. 2011; 7:2284–2295.
54. Jo S, Kim T, Im W. Automated Builder and Database of Protein/Membrane Complexes for Molecular Dynamics Simulations. *PloS ONE*. 2007; 2(9):e880. [PubMed: 17849009]
55. Dalke HW, Schulten K. VMD – Visual Molecular Dynamics. *J Mol Graphics*. 1996; 14:33–38.
56. Phillips JC, Braun R, Wang W, Gumbart J, Tajkhorshid E, Villa E, Chipot C, Skeel RD, Kale L, Schulten K. Scalable molecular dynamics with NAMD. *J Comput Chem*. 2005; 26:1781–1802. [PubMed: 16222654]
57. Hornak V, Abel R, Okur A, Strockbine B, Roitberg A, Simmerling C. Comparison of Multiple Amber Force Fields and Development of Improved Protein Backbone Parameters. *Proteins*. 2006; 65:712–725. [PubMed: 16981200]
58. Wang J, Wolf RM, Caldwell JW, Kollman PA, Case DA. Development and Testing of a General Amber Force Field. *J Comput Chem*. 2004; 25:1157–1174. [PubMed: 15116359]
59. Rosso L, Gould IR. Structure and Dynamics of Phospholipid Bilayers Using Recently Developed General All-Atom Force Fields. *J Comput Chem*. 2008; 29:24–37. [PubMed: 17910006]
60. Wang J, Wang W, Kollman PA, Case DA. Automatic atom type and bond type perception in molecular mechanical calculations. *J Mol Graph Model*. 2006; 25:247–260. [PubMed: 16458552]
61. Frisch, MJ.; Trucks, GW.; Schlegel, HB.; Scuseria, GE.; Robb, MA.; Cheeseman, JR.; Montgomery, JA., Jr; Vreven, T.; Kudin, KN.; Burant, JC.; Millam, JM.; Iyengar, SS.; Tomasi, J.; Barone, V.; Mennucci, B.; Cossi, M.; Scalmani, G.; Rega, N.; Petersson, GA.; Nakatsuji, H.; Hada, M.; Ehara, M.; Toyota, K.; Fukuda, R.; Hasegawa, J.; Ishida, M.; Nakajima, T.; Honda, Y.; Kitao, O.; Nakai, H.; Klene, M.; Li, X.; Knox, JE.; Hratchian, HP.; Cross, JB.; Bakken, V.; Adamo, C.; Jaramillo, J.; Gomperts, R.; Stratmann, RE.; Yazayev, O.; Austin, AJ.; Cammi, R.; Pomelli, C.; Ochterski, JW.; Ayala, PY.; Morokuma, K.; Voth, GA.; Salvador, P.; Dannenberg, JJ.; Zakrzewski, VG.; Dapprich, S.; Daniels, AD.; Strain, MC.; Farkas, O.; Malick, DK.; Rabuck, AD.; Raghavachari, K.; Foresman, JB.; Ortiz, JV.; Cui, Q.; Baboul, AG.; Clifford, S.; Cioslowski, J.; Stefanov, BB.; Liu, G.; Liashenko, A.; Piskorz, P.; Komaromi, I.; Martin, RL.; Fox, DJ.; Keith, T.; Al-Laham, MA.; Peng, CY.; Nanayakkara, A.; Challacombe, M.; Gill, PMW.; Johnson, B.; Chen, W.; Wong, MW.; Gonzalez, C.; Pople, JA. Gaussian 03, Revision C.02. Wallingford CT: Gaussian, Inc.; 2004.
62. Dupradeau FY, Cezard C, Lelong R, Stanislawiak E, Pecher J, Delepine JC, Cieplak P. R.E.DD.B.: A database for RESP and ESP atomic charges, and force field libraries. *Nucleic Acids Res*. 2008; 36:D360–D367. [PubMed: 17962302]
63. Pastor RW, Brooks BR, Szabo A. An analysis of the accuracy of Langevin and molecular dynamics algorithms. *Mol Phys*. 1998; 65:1409–1419.
64. Darden T, York D, Pedersen L. Particle mesh Ewald: An N-log(N) method for Ewald sums in large systems. *J Chem Phys*. 1993; 98:10089–10092.
65. Smart O, Goodfellow J, Wallace B. The pore dimensions of Gramicidin A. *Biophys J*. 1993; 65:2455–2460. [PubMed: 7508762]

**Figure 1.**

(a) Initial cytoplasmic view of EmrD from the apo-a simulation with helix numberings and locations of the N-ter (blue) and C-ter (red). (b) Image of EmrD with periplasm and cytoplasm labeled and a ruler indicating approximate z positions along the protein. Change in the separations of the helices between the last 1 ns and the first 1 ns of the (c) apo-a and (d) apo-b simulations. The diagonal elements are all equal to 0, the elements above the diagonal black line are the changes in separation between the cytoplasmic ends of the helices, and the elements below are the changes in separation between the periplasmic ends of the helices.

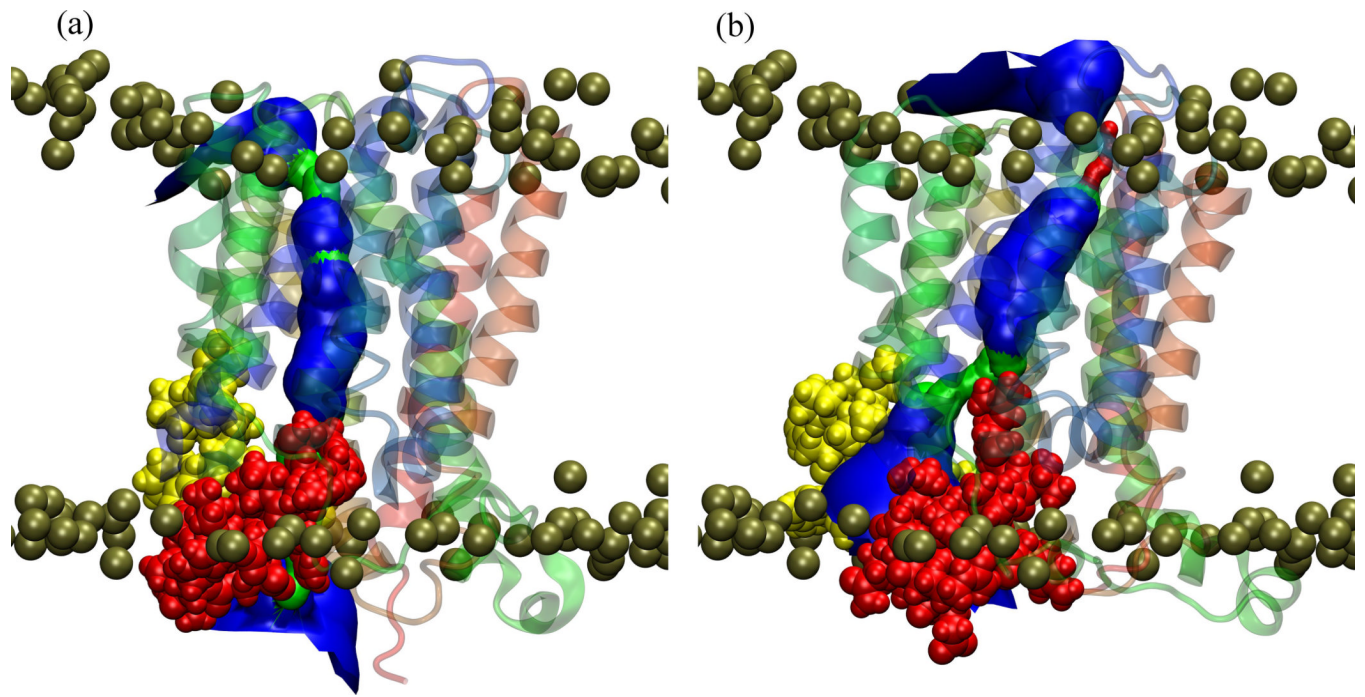


Figure 2.

EmrD conformation at the beginning (a) and the end (b) of the apo-a simulation, with central cavity profiles. Cavity profiles are colored red (radius < 1.15 Å), green (radius between 1.15 Å and 2.30 Å) and blue (radius > 2.30 Å). Residues 252 to 266 are shown as yellow spheres. Residues in the “selectivity filter” are shown as red spheres. The brown spheres represent lipid phosphorous atoms.

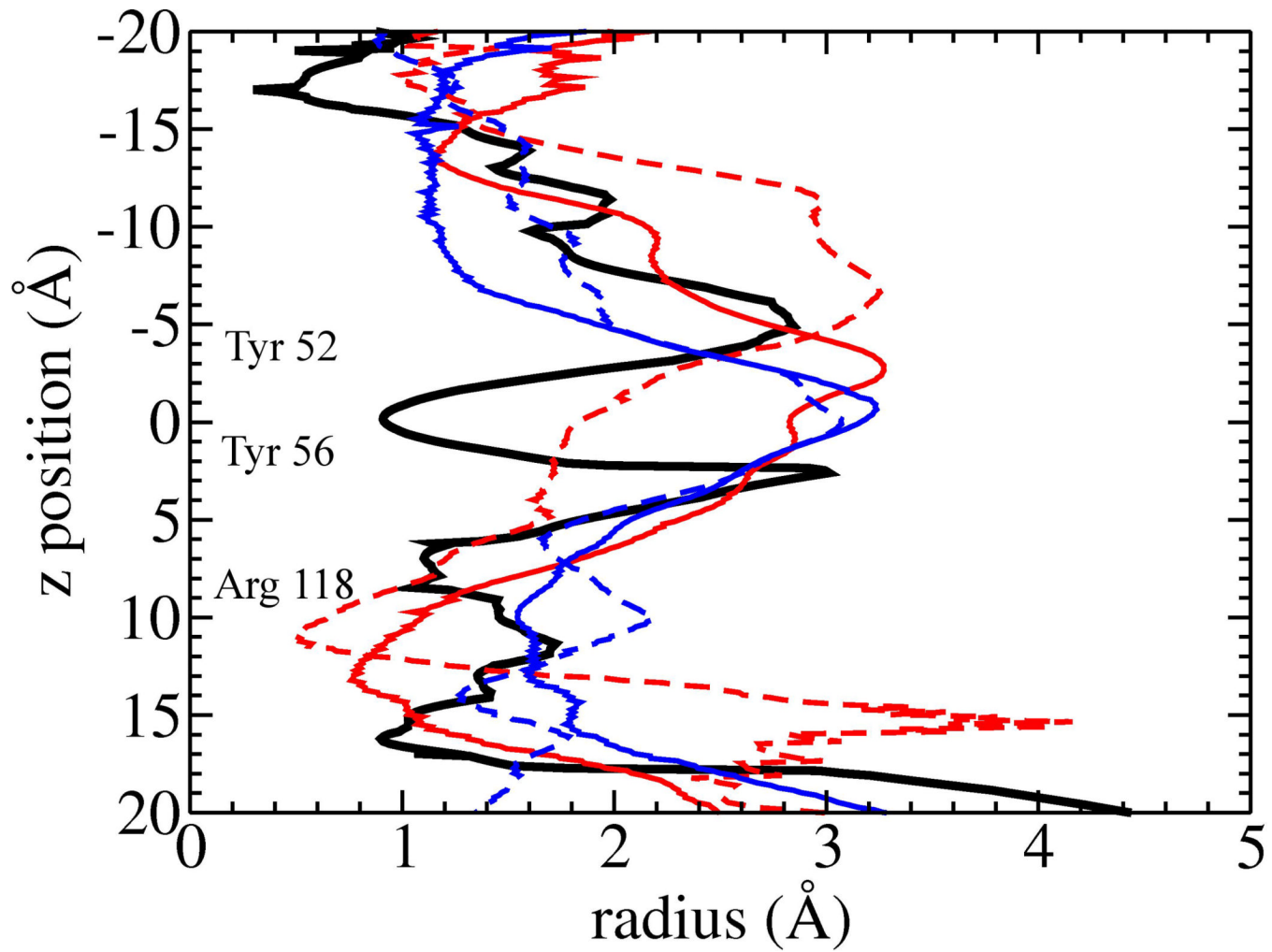
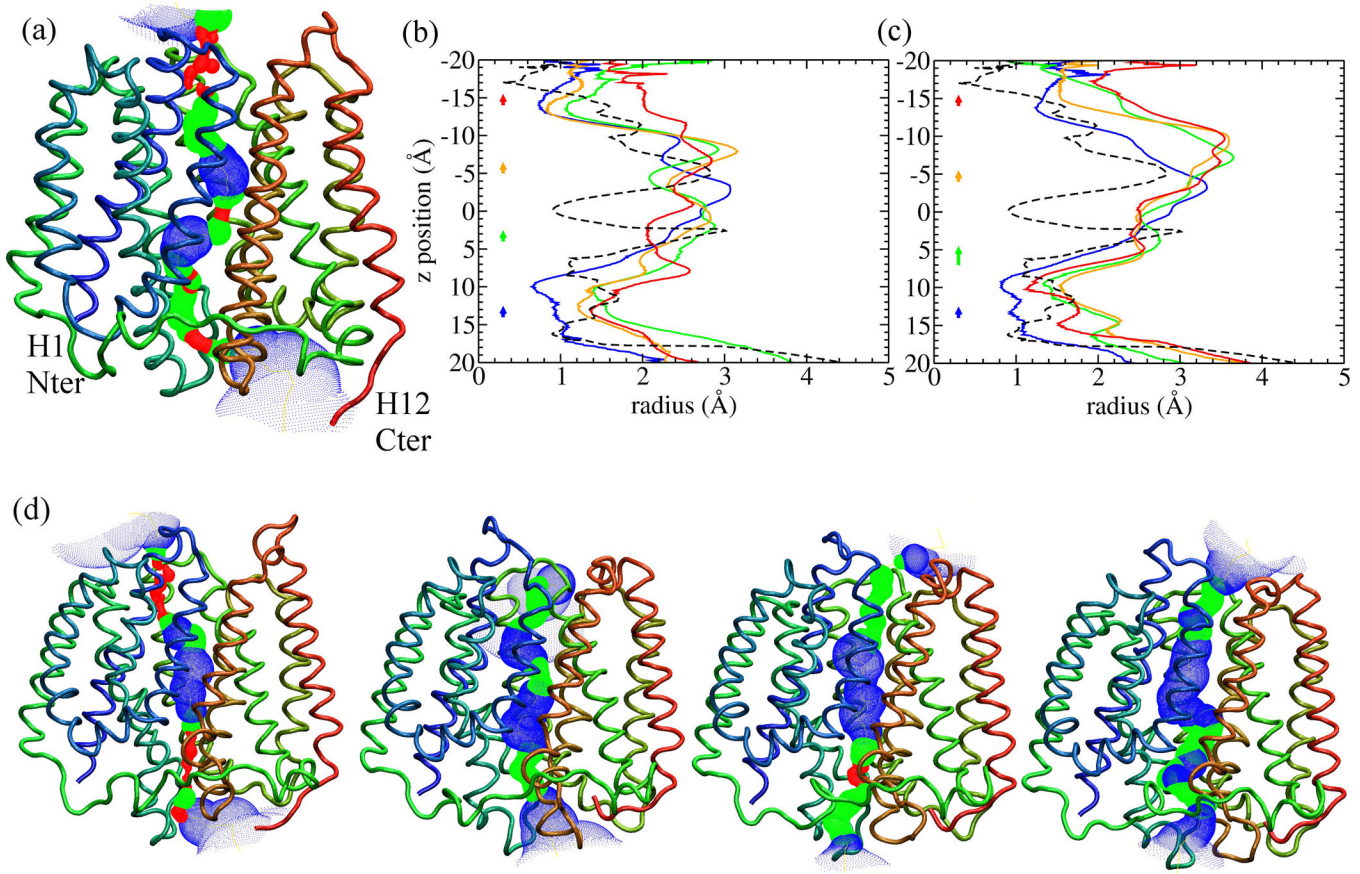
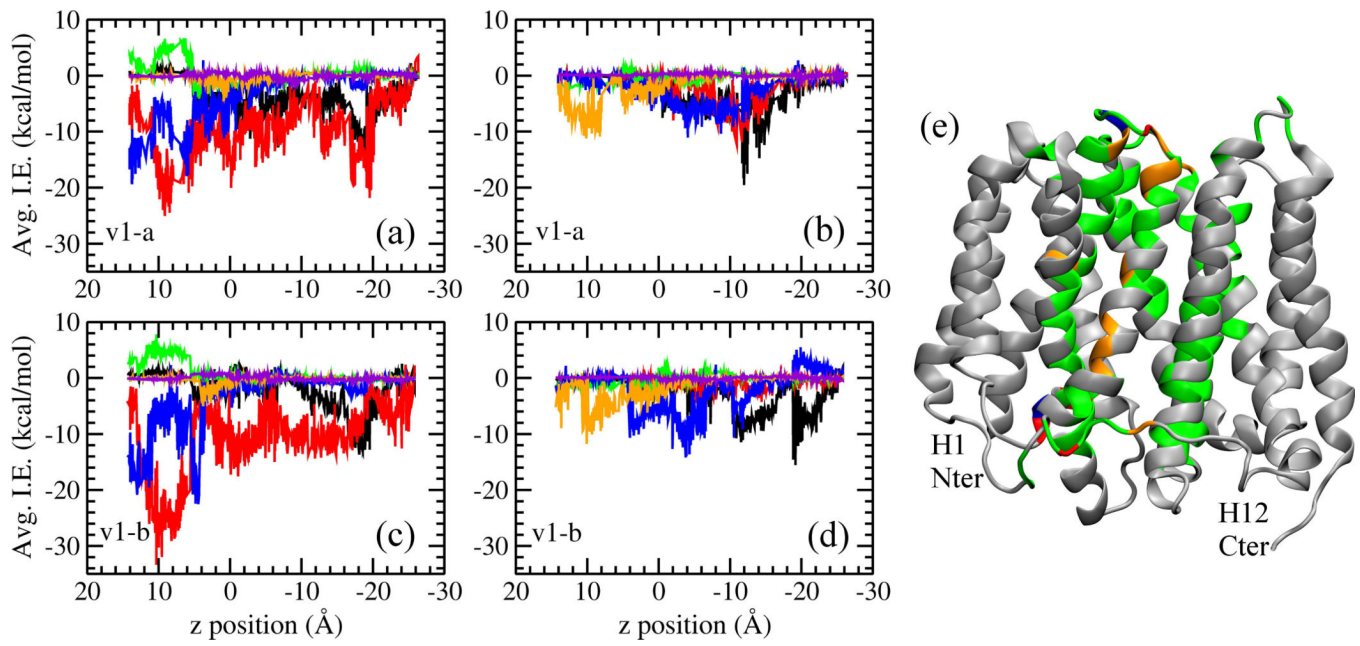


Figure 3.

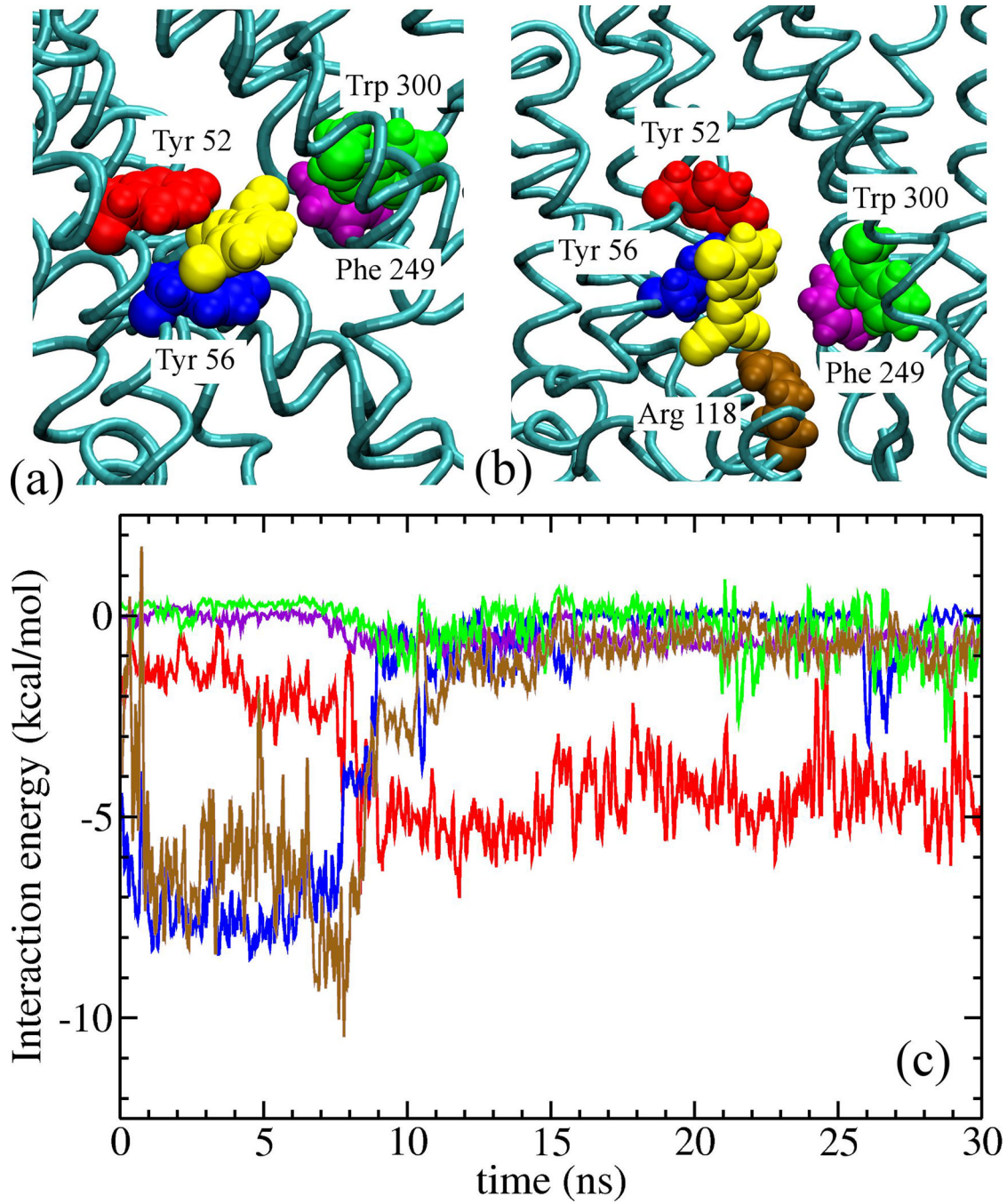
Radius of the central cavity of EmrD from the apo simulations. The red solid and dashed curves are an average over trajectory snapshots of the central cavity radius from the first 1 ns and the last 1 ns of the apo-a simulation respectively. The blue solid and dashed curves are the same but for the apo-b simulation. The black solid curve is the x-ray profile. The approximate positions of Tyr 52, Tyr 56, and Arg 118 are indicated.

**Figure 4.**

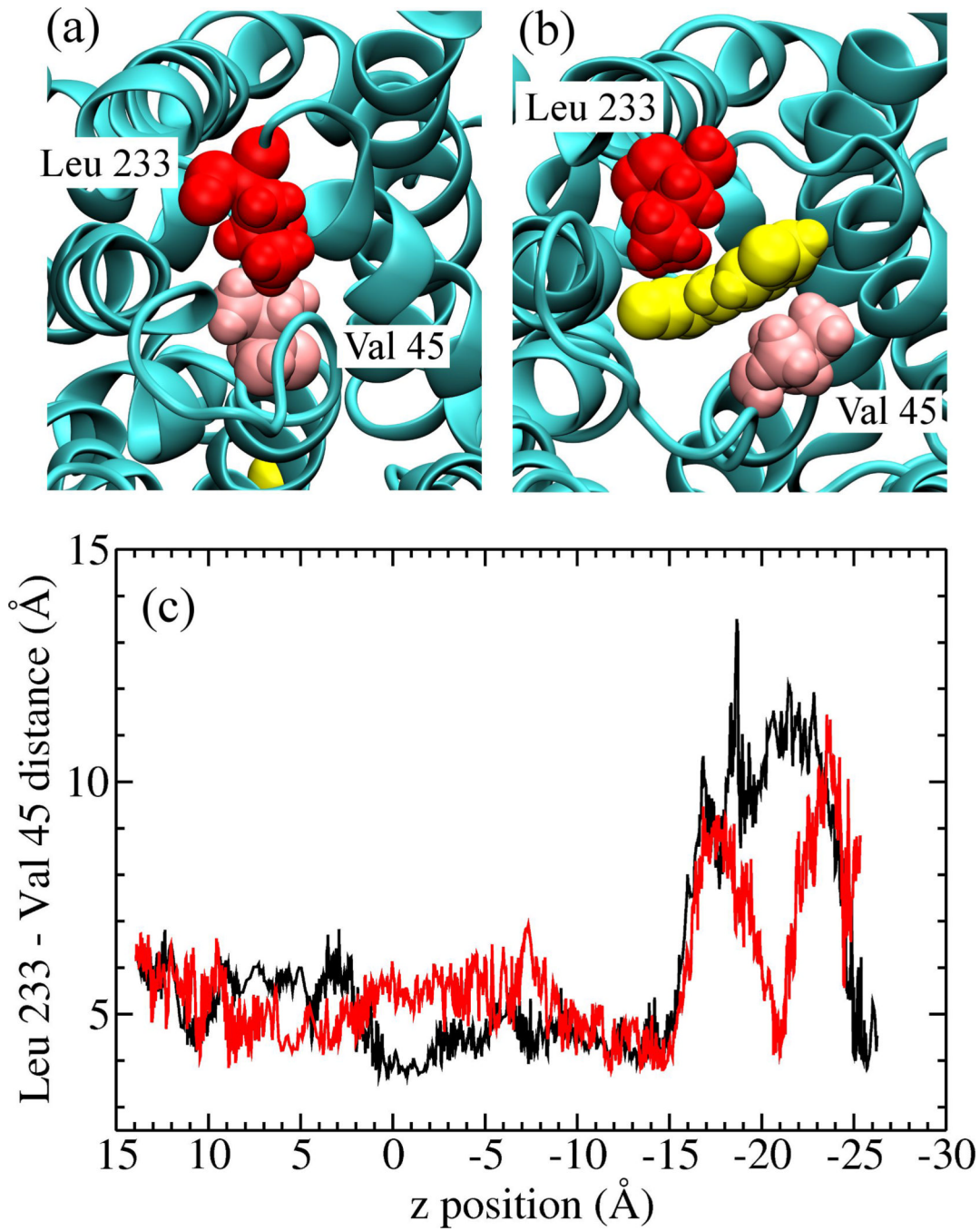
Conformational changes upon translocation. (a) Cavity profile for the EmrD x-ray structure aligned with the black dashed curve in (b) and (c). Average cavity radius (taken over 1 ns), at several intervals of the simulation, for v1-a (b) and v1-b (c). For each figure the time-evolution goes in order as blue, green, orange and red. The corresponding colored arrows on the vertical axis show the motion of the center of mass of CCCP while each average radius profile is obtained. (d) Cavity profile obtained from HOLE for four representative frames from v1-a corresponding to the blue, green, orange and red curves (left to right, respectively). Cavity profiles are colored red (radius < 1.15 Å), green (radius between 1.15 Å and 2.30 Å) and blue (radius > 2.30 Å). The coloring of helices is the same as in Fig. 1 a.

**Figure 5.**

Interactions of CCCP (vdW and electrostatic) with each of the helices, H1–H12 for both the v1-a (a and b) and v1-b (b and c) simulations as a function of the position of CCCP's center of mass. (a) and (c) show the N-domain helices H1–H6 (black, red, green, blue, orange and violet respectively). (b) and (d) show the C-domain helices H7–H12 (black, red, green, blue, orange and violet respectively). (e) EmrD colored by interaction energy with CCCP. Blue, green, orange and red correspond to average interaction energies greater than 0 kcal/mol, between 0 and -3 kcal/mol, -3 to -6 kcal/mol, and below -6 kcal/mol respectively. Grey coloring means that CCCP never came within a 3 Å cutoff distance from that region of the protein.

**Figure 6.**

Interactions within the central cavity observed in fs-a. Tyr 52 (red), Tyr 56 (blue), Phe 249 (purple), Trp 300 (green), Arg 118 (brown) and CCCP (yellow). (a) nearly parallel ring stacking of the aromatic rings of Tyr 52, Tyr 56 and CCCP. (b) the aromatic ring of CCCP interacting with the side chain of Tyr 56, while the nitrile groups interact with the Arg 118 side chain. Figure (c) shows interaction energies between the five residues pictured and CCCP, with same coloring as in (a) and (b).

**Figure 7.**

Motion of Leu 233 (located on H7–H8 loop, red) and Val 45 (located at periplasmic end of H2, pink) as CCCP (yellow) passes into the periplasmic space observed in v1-a. (a) initial snapshot, and (b) as CCCP is passing out of the central cavity. (c) Distance between the methyl carbon atoms of the side chains of Leu 233 and Val 45 as a function of the z position of the center of mass of CCCP as it moves from the cytoplasmic side (left) to the periplasmic side (right) of EmrD. The black and red curves in (c) correspond to v1-a and v1-b, respectively.

Table I

List of simulations

Simulation Name	Duration (ns)	With CCCP	Pulling Speed (Å/ns)	CCCP Position
apo-a	76	No	–	–
apo-b	50	No	–	–
v1-a	42.5	Yes	1	Cytoplasmic entrance
v1-b	42.5	Yes	1	Cytoplasmic entrance
fs-a	30	Yes	–	Cytoplasmic side of cavity, snapshot from v1-a
fs-b	30	Yes	–	Central cavity, snapshot from v1-a
fs-c	30	Yes	–	Periplasmic side of cavity, snapshot from v1-a

CCCP average interaction energies (kcal/mol) with EmrD residues.

Residue	v1-a	v1-b	fs-a	fs-b	fs-c
Asp 190	-19.3 ± 5.9	-21.1 ± 7.0	*	*	*
Asp 68	-6.8 ± 1.6	-8.3 ± 1.6	*	*	*
Arg 118	-7.0 ± 4.5	-5.6 ± 4.9	-6.7 ± 2.4	*	*
Gln 60	-3.8 ± 1.8	-5.0 ± 2.4	-2.7 ± 1.3	*	*
Tyr 56	-4.4 ± 2.1	-3.9 ± 2.0	-6.1 ± 2.4	-3.1 ± 2.3	*
Trp 300	-2.1 ± 0.53	-1.2 ± 0.59	-2.0 ± 0.96	-1.7 ± 0.21	*
Phe 249	-1.1 ± 0.74	-0.55 ± 0.49	-0.73 ± 0.34	-0.98 ± 0.29	*
Gln 21	-3.1 ± 1.5	-2.8 ± 0.80	-1.0 ± 1.4	-1.9 ± 1.1	*
Tyr 52	-3.6 ± 1.9	-3.1 ± 2.4	-4.1 ± 1.7	-2.1 ± 1.2	-1.7 ± 0.53
Gln 24	-3.8 ± 2.0	-1.2 ± 1.5	-3.2 ± 1.7	-4.0 ± 1.4	*
Met 49	-2.4 ± 1.0	-2.4 ± 1.5	-1.8 ± 0.67	-2.1 ± 0.74	-3.3 ± 1.5
Glu 227	-2.8 ± 3.7	-2.1 ± 1.8	-	-1.9 ± 1.5	-6.3 ± 3.3
Asp 292	-1.3 ± 0.86	-7.0 ± 2.5	*	*	-8.6 ± 1.4
Gln 46	-0.70 ± 0.45	-	*	*	-2.4 ± 0.90
Val 45	-3.2 ± 1.4	-2.6 ± 1.3	*	*	-2.6 ± 1.5
Leu 233	-2.8 ± 1.5	-3.3 ± 1.6	*	*	-1.5 ± 0.62

(-) no interactions observed.

(*) no interactions observed due to the initial location of CCCP in the force free simulation. Standard deviations represent the sizes of fluctuations in the interaction energy around the mean value.

Table II